Capacitive Skin Sensors for Robot Impact Monitoring

Samson Phan, Zhan Fan Quek, Preyas Shah, Dongjun Shin, Zubair Ahmed, Oussama Khatib, and Mark Cutkosky

Abstract—**A new generation of robots is being designed for human occupied workspaces where safety is of great concern. This research demonstrates the use of a capacitive skin sensor for collision detection. Tests demonstrate that the sensor reduces impact forces and can detect and characterize collision events, providing information that may be used in the future for force reduction behaviors. Various parameters that affect collision severity, including interface friction, interface stiffness, end tip velocity and joint stiffness irrespective of controller bandwidth are also explored using the sensor to provide information about the contact force at the site of impact. Joint stiffness is made independent of controller bandwidth limitations using passive torsional springs of various stiffnesses. Results indicate a positive correlation between peak impact force and joint stiffness, skin friction and interface stiffness, with implications for future skin and robot link designs and post-collision behaviors.**

I. INTRODUCTION

As humans and robots begin to share the same workspace, their safe interaction is increasingly important. Previous research has shown that compliant coverings can reduce impact forces to below dangerous levels [1]. Such coverings, in addition to providing energy and impact absorption, can also provide touch capability. In this work, a skin containing capacitive touch sensors is evaluated for its ability to detect collisions and to reduce impact forces. In comparison to approaches involving capacitive proximity sensing (e.g., [2]), the sensors here are covered with a flexible outer shield to minimize their capacitive coupling with nearby objects. Numerous examples of capacitive touch sensors are reported in the literature, along with commercial examples (e.g. [3]). The sensor used for these experiments is adapted from a design reported in [4], selected for its combination of robustness, low cost and sensitivity to light contacts.

For the intended application, the skin and sensors need to be durable, robust and able to measure collisions of varying intensity. For practical reasons, the skin cannot easily be made thick enough that the robot has time to utilize information obtained from force and skin sensors during a collision to significantly reduce the severity of the initial impact [5]. However, we believe that a human-safe robot should be aware of all intentional and unintentional contacts, including where they occur and the nature of the contact (e.g. whether concentrated or distributed, and stationary or sliding).

Previous work has investigated compliant coverings as part of a solution for a human-safe robot [6]. Several researchers have attempted to provide robots with proprioception while reducing impact forces. In [7] a viscoelastic compliant covering is integrated with an optical contact detection system, which has the advantage of being immune to electromagnetic disturbances, common in robotic environments. In [8], a highly scalable and flexible skin sensor is reported, capable of covering a large area at desired sensor densities. Such imaging based methods, however, typically require greater processing, which reduces bandwidth. Another compliant design [9] utilizes encapsulating air bladders outfitted with pressure sensors to reduce impact force as well as detect collision. Inherent with this design is a relatively low taxel density along one dimension.

Other methodologies to reduce impact forces during human robot collisions have sought to minimize the inertia and stiffness of the arm to reduce the amount of energy transfer during a collision [10], [11]. However, others have argued that in the event of a high-speed collision, the drivetrain stiffness and motor inertia have a limited effect since the main factors are the link inertia and skin thickness [12].

With these considerations in mind, we developed a moderately thick (10 mm) skin for the Stanford human-safe arm. The design considerations include trade-offs between desired spatial resolution for resolving contacts and the number of sensors, achievable data rates, and the thickness and sensitivity of the skin. Ideally, the skin and sensors should have a sufficient sampling rate and dynamic response that temporal details of the contact are available, including the details of rapid contacts as would occur during a collision.
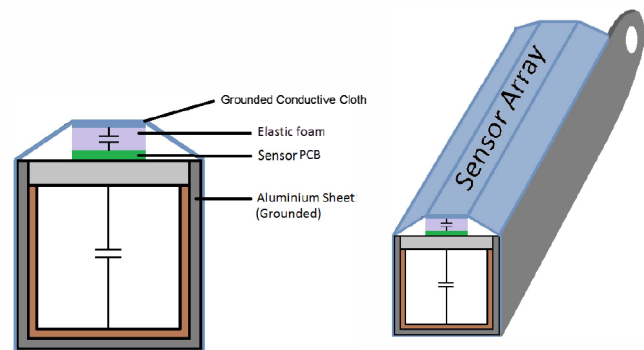

Fig. 1. Skin sensor and prototype link schematic. Compression of the elastic foam changes the capacitance of each element, altering its oscillation frequency. A grounded foil backing prevents stray capacitance from affecting the signal. The sensors are arrayed along the length of the link.

We conducted tests using a passive prototype link mounted to the end of an industrial robot capable of end tip speeds up to 10 m/s (Figure 1). The passive link is attached to the robot with a revolute joint that has a known torsional stiffness and damping. This setup is meant to approximate the behavior of one link of the Stanford Human-Safe arm, without subjecting

the actual prototype to potentially damaging impacts.

As a "worst case" collision scenario, the link is made to collide with a rigidly fixed 3 inch diameter steel cylinder that is coated to alter friction and compliance for various experimental parameters. Forces and moments at the attachment point where the link is mounted to the robot are recorded using a commercial force/torque sensor (JR3 Inc., Woodland, CA) along with the rotation of the link before and after the collision. Eight capacitive sensors, using a design adapted from [4], are arrayed in a line where they will be subjected to impact.

Specific questions that we sought to answer from our collision experiments are:

1) Can a skin sensor provide impact force detection comparable to a joint torque sensor?
2) Can a skin sensor provide useful contact location information, along with the distribution of forces?
3) How does joint stiffness affect sensor behavior?
4) How do interface stiffness and friction affect skin sensor data?

II. IMPACT MODEL

The collision can be modeled as a two link system with Link 1 (most distal) and Link 2 connected by a torsional spring. Link 1 interacts with a rigid wall with a force proportional to the deflection, q_1, and is connected to Link 2 by an ideal torsional spring whose force is proportional to $q_1 - q_2$. Link 2 rotates at a fixed rate ($\ddot{q}_2 = 0$).
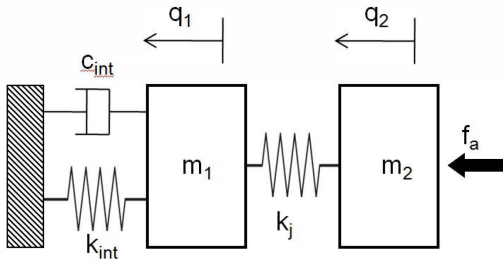

Fig. 2.   A schematic of the system

Variable	Definition	Units
k_{int}	Interface Stiffness	N/m
k_j	Joint Stiffness	N/m
m_1	Mass of Link 1	kg
m_2	Mass of Link 2	kg
f_a	Applied Force	N
$\dot{q}_0$	Initial Velocity	m/s
c_{int}	Damping Term	Ns/m

TABLE I
VARIABLES FOR IMPACT MODEL

The equations of motion for Link 1 and Link 2 are as follows:

$$m_1\ddot{q}_1 = -(k_{int} + k_j)q_1 + k_j q_2 - c_{int}\dot{q}_1 \qquad (1)$$

$$m_2\ddot{q}_2 = f_a + k_j(q_1 - q_2) \qquad (2)$$

The interface is modeled as a Kelvin-Voigt model, a commonly used model for foam. This model is used to approximate the hysteretic effect from the foam as well as frictional losses associated with the contact. Ideally, when the position error for m_2 is 0, then $f_a = 0$. For an infinitely stiff joint, ($k_j = \infty$), our system behaves as a 1DOF underdamped system, whose natural frequency is $w_0 = \sqrt{k_{int}/(m_1 + m_2)}$ and damped natural frequency is $w_d = w_0\sqrt{1 - \zeta^2}$, where $\zeta = c_{int}/2\sqrt{(m_1 + m_2)k_{int}}$. The solution is

$$q = \frac{\dot{q}_0}{w_d}e^{-\zeta w_\bullet t}sin(w_d t) \qquad (3)$$

Conversely, for an infinitely compliant joint $k_j = 0$, the solution is slightly altered, with $w_0 = \sqrt{k_{int}/(m_1)}$ and $\zeta = c/\sqrt{2m_1 k_{int}}$. The solution has the form of equation 3 during the impact period. In the coupled case (for finite k_j) one expects higher skin deflections and longer contact times. In addition, for the case of high friction, one expects higher peak forces and shorter contact times. These expected effects are summarized in Table II.

Variable	Impact Duration	Peak Force
Joint Stiffness	↓	↑
Skin Friction	↓	↑
Interface Stiffness	↓	↑

TABLE II
EXPECTED EFFECTS OF TEST PARAMETERS
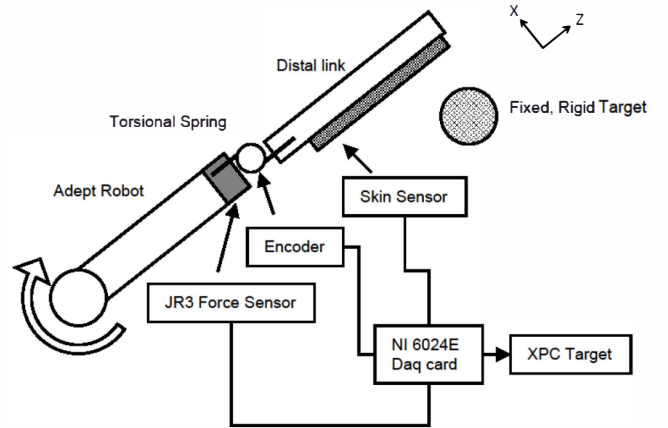
III. EXPERIMENTAL SETUP

Fig. 3.   Schematic of experimental setup.

A. Physical setup

An Adept robotic manipulator is equipped with an additional passive link covered with a compliant skin sensor, as shown in figure 5. Torsional springs of varying stiffness are mounted at the joint as a passive means of providing stiffness, separating controller bandwidth issues from ideal behavior. The primary axis velocity of the Adept robot is controlled; all other joints are held fixed. The arm trajectory is designed
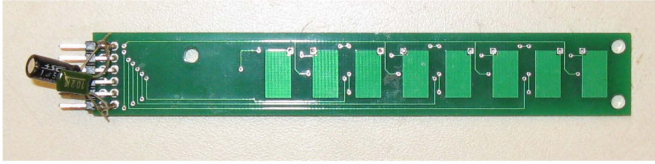
Fig. 4. PCB of skin sensor. The skin sensor consists of 8 capacitive nodes seen here with the elastic foam and outer conductive cloth removed. The sensors are arranged linearly along the link. Each node consists of a 5 x 10 mm taxel with 5 mm spacing.

to initiate contact at Sensor 3. Robot movement ceases when the center of contact is at Sensor 7 via a preplanned position controller. The center of contact moves distally during the test.

Eight capacitive sensors are mounted on a PCB (Fig. 4) and covered with layers of silicone rubber foam and conductive rubber and cloth. The design and quantitative characterization of the sensors are discussed in [4]. Briefly, the sensors have a range of 0-100 N per taxel, with a minimum resolvable force of approximately 0.02 N and a flat frequency response to 80 Hz, due to the low hysteresis of the silicone rubber dielectric.
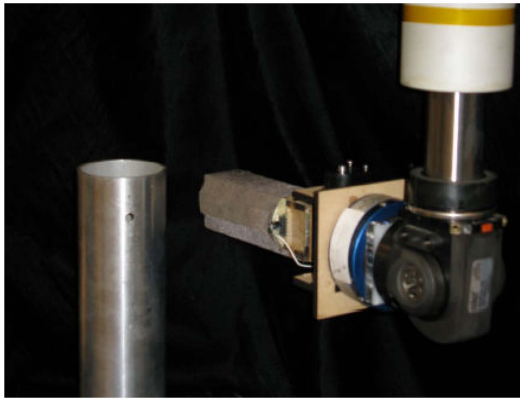

Fig. 5. Picture of experimental setup. The sensorized link attached to the Adept robot (right) is about to impact the target cylinder (left).

B. Target

The arm collides with a rigidly fixed 3 inch diameter steel cylinder. The diameter was chosen to mimic a forearm, a body part likely to be impacted by a robot, and which has been chosen as an unintended robot target by other researchers [13]. The use of a steel cylinder is clearly a "worst case" scenario, being much stiffer than a human arm and incapable of moving. Softer collisions are achieved by adding pieces of foam to the outside of the cylinder. Compliant coverings were chosen with stiffness of muscle tissue and bone in mind [14],[15],[16]. The effective stiffness can be modeled as

$$k_{int} = 1/(1/k_s + 1/k_t) \qquad (4)$$

where k_s and k_t are the skin and target stiffness, respectively.

Additionally, interface friction was varied using surface coatings (masking tape or 400 grit sandpaper). This method allowed indepedent variation of interface friction and interface

stiffness. These surfaces were chosen to closely mimic the bounds of in vivo skin friction values [17].

C. Data and Data Acquisition

A USDigital optical incremental encoder is attached to the joint to detect deflection angles. A JR3 6 axis force and moment sensor is attached proximally to the joint to detect transmitted forces and moments. Data from the compliant skin sensor, located on the impacting surface of the arm, are converted to an analog signal before being acquired on a National Instrument PCI-6024E data acquisition card, which is installed on a computer runnning XPC. Data were acquired and processed in Matlab at 3.33 Khz (skin sensor) and 10 Khz (JR3).

Variable	Levels	Units
End Tip Velocity	0.9, 3.4, 6.3	m/s
Joint Stiffness	1.591, 27.793	Nmm/deg
Skin Friction	0.3, 0.6	
Interface Stiffness	150, 600	N/m

TABLE III
EXPERIMENTAL TEST SETTINGS
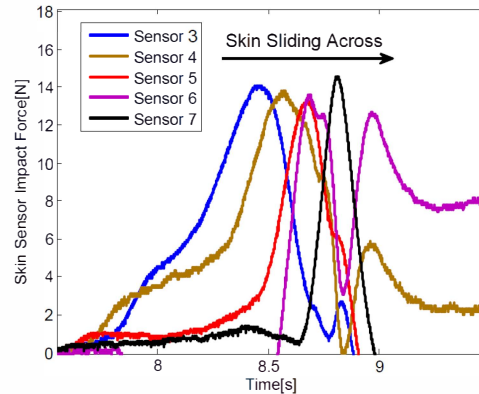
IV. RESULTS

A. Skin sensor

Fig. 6. Skin sensor data, depicting initial collision followed by sliding of the arm across target (high stiffness, medium velocity case, collision at 4m/s)

Figure 6 shows data collected from the skin sensor during a collision test. The collision initially occurs at sensor 3, and the point of contact slides across the surface, triggering sensor 4 through 7 sequentially. Sensors 1,2 and 8 are not contacted during the entire collision phase and do not show a force change. The skin sensor is therefore able to provide both spatial and temporal information on the contact forces during a collision.

For simplicity, the following plots sum the sensor force and moment data for comparison with readings from the force/torque sensor, resolved to the passive joint of the sensorized link:

$$f_{tot}(t) = \sum_{i=1}^{8} f_i(t) \qquad (5)$$

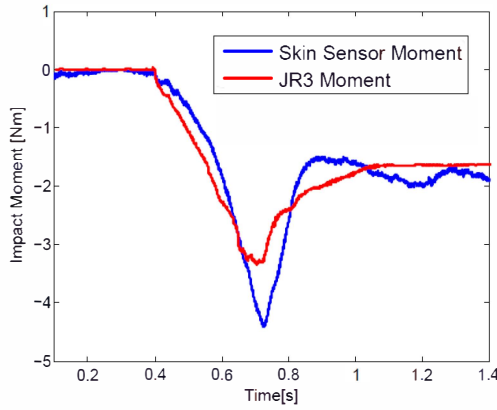$$m_{tot}(t) = \sum_{i=1}^{8} f_i(t) * l_i \qquad (6)$$

Fig. 7. Total moment obtained using the skin sensors and force/torque sensor for a high stiffness, 3.4 m/s. The profiles are similar, with some difference due to the distal link inertia. After peak, the recorded moment decreases to a steady state value. This is a result of the joint stiffness forcing the link into the target.

Figure 7 shows the data obtained via equation 6, together with the corresponding moment measured at the force/torque sensor. It can be seen that the skin sensor has sufficient responsiveness to record overall contact forces during the collision event.
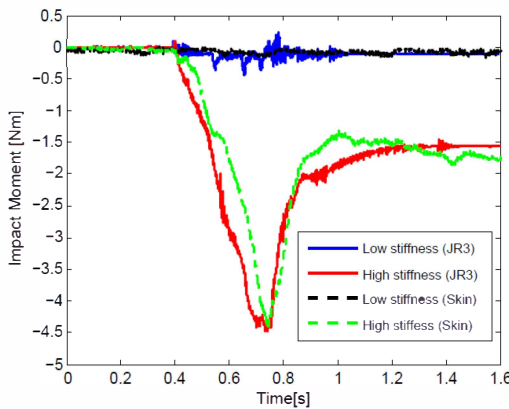
B. Joint stiffness effect

Fig. 8. A higher impact moment is recorded for both the JR3 and the skin for the collision experiment with higher joint stiffness for collisions at 3.4m/s.

Figure 8 shows that joint stiffness is positively correlated to skin sensor readings and moment data from the force/torque sensor; low stiffness provides little skin deformation and a correspondingly low force.

C. Skin friction effect

Figure 9 shows the measured impact moment from the force/torque sensor and the impact force from the skin sensor

(a) Impact moment for different skin friction values

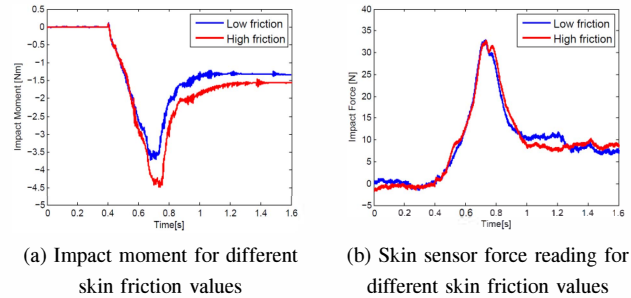(b) Skin sensor force reading for different skin friction values

Fig. 9. (a) A higher impact moment from the JR3 sensor is obtained for the collision experiment with higher skin friction. This is due to the addition of the friction force which acts tangentially to the skin sensor surface. (b) The skin sensor registers similar impact forces for both collision tests, as it detects only normal forces.
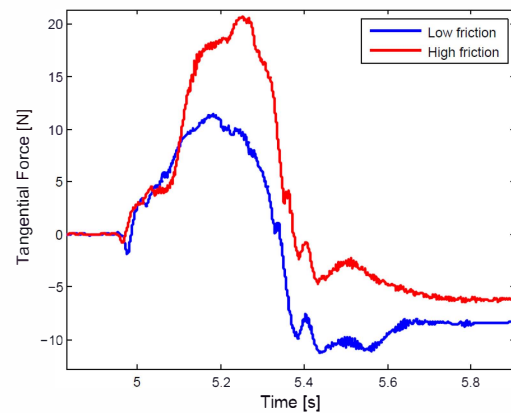

Fig. 10. JR3 force sensor data during collision. High friction skin induces higher tangential forces throughout contact.

under varying friction conditions. While increased friction increases the measured moment in a manner similar to increased velocity or stiffness, the skin sensor provides a relatively consistent reading for high and low friction conditions. This observation is born out by Figure 10, which shows the tangential force obtained through transformation of the force data along the joint. Thus a combination of skin and force/torque sensing can distinguish among these effects.

D. Interface stiffness effect

Figure 11 shows the effects of different interface stiffness, obtained by covering the metal pole with a compliant covering. Note that the larger force recorded by the skin sensor at steady state in this case is because the compliant covering on the pole effectively increases the deflection of the link at steady state, resulting in a greater steady state force.

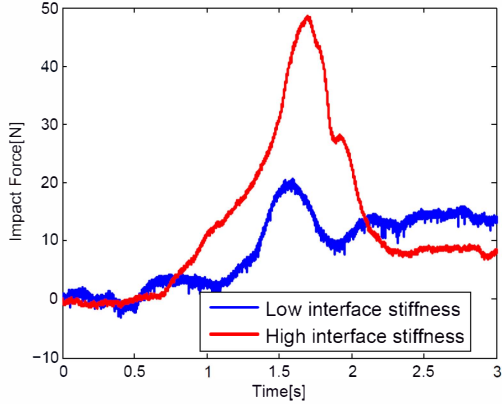The results for each of the robot parameters are summarized in Table IV.

Fig. 11. The skin sensor registers a higher impact force for the collision experiment with higher interface stiffness. The higher steady state force for the low interface stiffness case is due to the addition of the compliant covering over the metal pole, which leads to higher joint deflection, and hence higher force.

Variable	Impact duration	Peak Impact
Joint Stiffness	↑	↑
Skin Friction	—	↑
Interface Stiffness	—	↑

TABLE IV
TEST PARAMETER EFFECTS

V. DISCUSSION

A. Skin sensor

The skin sensor can provide an accurate description of dynamic forces at the contact. As seen in the figures, the skin sensor and force/torque sensor report similar peak forces with the same timing. In addition, the skin sensor provides a spatial description of the contact. This increase in sensory perception may allow for more complex reaction behaviors.

Changes in force measured by a skin sensor element can occur for 2 reasons: The epicenter of contact is passing over the center of the node, or there is a greater deflection. This information, coupled with joint sensor data, can be used to determine the type of collision, whether it be normal, oblique, or consist of multiple contacts. One can track the collision point on the surface using the time differences between the peaks in sensor force readings. A 2D array of sensors would be able to provide the center of contact on a plane.

B. Joint stiffness effect

In these experiments, distal joint stiffness plays an important role in the collision dynamics. As shown in Figure 8, the peak impact force and moment are significantly higher for the high joint stiffness case compared to the low joint stiffness case. As the collsion forces were quite low during the low stiffness collsion test, it is difficult to perform contact time analysis. One would expect shorter contacts for low stiffness due to less inertial coupling. Collision detection and reaction schemes, such as a switch to compliance control mode after collision detection, which effectively reduces the joint stiffness, may

be useful in reducing the post-collision force experienced by a victim being pushed into a rigid surface (e.g the clamped condition). The impact detection can be provided by the skin sensor.

C. Interface friction effect

Different friction cases show similar contact times and normal force profiles from the skin sensor. However, higher forces due to friction affect the impact moment, as seen in Figure 10. A low friction surface increases the angle of contact, making for a more "glancing" blow. Reference [18] showed that the interface stiffness is related to the angle of contact β by the following relationship:

$$k_{int,\beta} = k_{int,\perp}(cos(\beta))^2 \tag{7}$$

A glancing blow effectively reduces interface stiffness, which lowers peak forces. The tangential force F_t is induced by the normal force F_n by the follwing equation.

$$F_t = \mu F_n \tag{8}$$

For a given configuration, lower friction would result in a lower maximum stress, decreasing the likelihood of injury. Newer robot designs can incorporate low friction skins as an inexpensive yet effective means of increasing robot performance without decreasing safety.

The Kelvin-Voigt based impact model does not accurately predict decreased natural frequency and increased collision forces as interface friction increases. Losses from interface friction and viscous damping may not be lumped together for an overall damping term.

D. Interface stiffness effect

From analysis of a 1 DOF spring damper system, it is apparent that the interface stiffness has a profound effect on the impact dynamics. These tests demonstrate the predicted results in Figure 11. This suggests that robotic platforms can be made safer by the addition of compliant coverings.

E. Interplay between skin and joint stiffness

Our skin sensor requires skin deflection in order to quantify an impact. This requires a certain amount of skin compliance. If the jont stiffness is too low however, $(k_{int} >> k_j)$, then a collision will not be detected by the skin sensor. This assumes that the link's inertia has little effect on collision dynamics, which is true for low joint velocities and lightweight links.

VI. SUMMARY OF DISCUSSION

We have demonstrated the efficacy of a capacitive skin sensor in collision detection and characterization. It provides dynamic contact information comparable to that from a joint torque sensor, while allowing contact location and force distribution along the skin to be obtained. Using the skin sensor and the torque sensor together, robot parameters affecting collision forces have also been explored, with the findings indicating that a higher joint stiffness, interface stiffness and skin friction lead to higher collision impact forces and hence a greater chance for injury.

VII. FUTURE WORK

The work here demonstrates the capacitive sensor's ability to accurately sense and locate an impact. Future research will involve extending the sensors to a two-dimensional array around each robot link and developing impact mitigation behaviors. These expanded arrays will encounter difficulties associated with interrogating large number of sensors. In addition to designing an efficient method to sample numerous sensors, optimal sensor density must be taken into consideration. Sensor density is predicted to be lower than areas where contact is expected and fine manipulation is necessary, such as fingertips.

Work has been done on post collision behaviors, and there has been considerable debate over what a robot should do after a collision has been detected [19]. Current protocols call for an immediate stop of all links, but there are scenarios in which this will not be the most appropriate reaction behavior. In the case of a robot collision with a human constrained against a wall, for example, the ISO mandated response of pausing would potentially lock or even squeeze the victim in place until help arrived.

This work demonstrates the performance of a compliant skin sensor optimized for providing a signal proportional to deflection. Future designs may be optimized for collision detection, as the proximity to the point of contact may allow the skin sensors to provide a faster response than traditional joint torque sensors through the use of local reflexive behavior.

The current model assumes a 1 dimensional collision that is unable to capture the effects of friction and angle of incidence. Future models will refine contact analysis to include such parameters. Such analysis will provide researchers with predictive abilities to determine peak forces in a collision using robot parameters such as joint configuration, end tip velocity, and interface stiffness. While this body of work provides general guidelines on robot design, it does not map exact parameter values to injury probability. Having identified various parameters that affect collision forces, future research will attempt to develop design tradeoff tools and optimization criteria for the design of a human-safe robot.

REFERENCES

[1] S. Haddadin, A. Albu-Schaffer, M. Strohmayr, M. Frommberger, and G. Hirzinger, "Injury evaluation of human-robot impacts," in *2008 IEEE International Conference on Robotics and Automation*. IEEE, May 2008, pp. 2203–2204.

[2] B. Mayton, L. LeGrand, and J. R. Smith, "An Electric Field Pretouch system for grasping and co-manipulation," in *2010 IEEE International Conference on Robotics and Automation*. IEEE, May 2010, pp. 831–838.

[3] P. P. Inc, "Pressure Profile RoboTouch Website." [Online]. Available: http://www.pressureprofile.com/products-robotouch

[4] J. Ulmen and M. Cutkosky, "A robust, low-cost and low-noise artificial skin for human-friendly robots," in *2010 IEEE International Conference on Robotics and Automation*. IEEE, May 2010, pp. 4836–4841.

[5] M. Zinn, O. Khatib, and B. Roth, "A new actuation approach for human friendly robot design," in *IEEE International Conference on Robotics and Automation, 2004. Proceedings. ICRA '04. 2004*. IEEE, 2004, pp. 249–254 Vol.1.

[6] G. Berselli and G. Vassura, "Differentiated layer design to modify the compliance of soft pads for robotic limbs," in *2009 IEEE International Conference on Robotics and Automation*. IEEE, May 2009, pp. 1285–1290.

[7] Y. Yamada, M. Morizono, U. Umetani, and T. Takahashi, "Highly Soft Viscoelastic Robot Skin With a Contact Object-Location-Sensing Capability," *IEEE Transactions on Industrial Electronics*, vol. 52, no. 4, pp. 960–968, Aug. 2005.

[8] Y. Ohmura, Y. Kuniyoshi, and A. Nagakubo, "Conformable and scalable tactile sensor skin for curved surfaces," in *Proceedings 2006 IEEE International Conference on Robotics and Automation, 2006. ICRA 2006*. IEEE, 2006, pp. 1348–1353.

[9] S. Jeong and T. Takahashi, "Impact Force Reduction of Manipulators Using a Dynamic Acceleration Polytope and Flexible Collision Detection Sensor," *Advanced Robotics*, vol. 23, no. 3, pp. 367–383, Jan. 2009.

[10] I. Sardellitti, O. Khatib, and Shin, "A hybrid actuation approach for human-friendly robot design," in *2008 IEEE International Conference on Robotics and Automation*. IEEE, May 2008, pp. 1747–1752.

[11] O. Khatib, M. Cutkosky, and D. Shin, "Design methodologies of a hybrid actuation approach for a human-friendly robot," in *2009 IEEE International Conference on Robotics and Automation*. IEEE, May 2009, pp. 4369–4374.

[12] S. Haddadin, A. Albu-Schaffer, and G. Hirzinger, "The role of the robot mass and velocity in physical human-robot interaction - Part I: Non-constrained blunt impacts," in *2008 IEEE International Conference on Robotics and Automation*. IEEE, May 2008, pp. 1331–1338.

[13] B. Povse, D. Koritnik, T. Bajd, and M. Munih, "Correlation between impact-energy density and pain intensity during robot-man collision," in *2010 3rd IEEE RAS & EMBS International Conference on Biomedical Robotics and Biomechatronics*. IEEE, Sep. 2010, pp. 179–183.

[14] M. Van Loocke, C. G. Lyons, and C. K. Simms, "Viscoelastic properties of passive skeletal muscle in compression: stress-relaxation behaviour and constitutive modelling." *Journal of biomechanics*, vol. 41, no. 7, pp. 1555–66, Jan. 2008.

[15] Y. Zheng, A. F. Mak, and B. Lue, "Objective assessment of limb tissue elasticity: development of a manual indentation procedure." *Journal of rehabilitation research and development*, vol. 36, no. 2, pp. 71–85, Apr. 1999.

[16] T. Keller, Z. Mao, and D. Spengler, "Youngs Modulus, Bending Strength, and Tissue Physical Properties of Human Compact Bone," *Bone*, vol. 8, no. 4, pp. 592–603, 1990.

[17] M. Zhang and A. F. T. Mak, "In vivo friction properties of human skin," *Prosthetics and Orthotics International*, vol. 23, no. 2, pp. 135–141, 1999.

[18] M. Zinn, O. Khatib, B. Roth, and J. Salisbury, "Playing it safe," *IEEE Robotics & Automation Magazine*, vol. 11, no. 2, pp. 12–21, Jun. 2004.

[19] S. Haddadin, A. Albu-Schaffer, A. De Luca, and G. Hirzinger, "Collision detection and reaction: A contribution to Safe Physical Human-Robot Interaction," in *2008 IEEE/RSJ International Conference on Intelligent Robots and Systems*. IEEE, 2008, pp. 3356–3363.